Volume 38 | Number 10 | October 2014 | Pages 4633–5098

NJC

New Journal of Chemistry

A journal for new directions in chemistry

www.rsc.org/njc

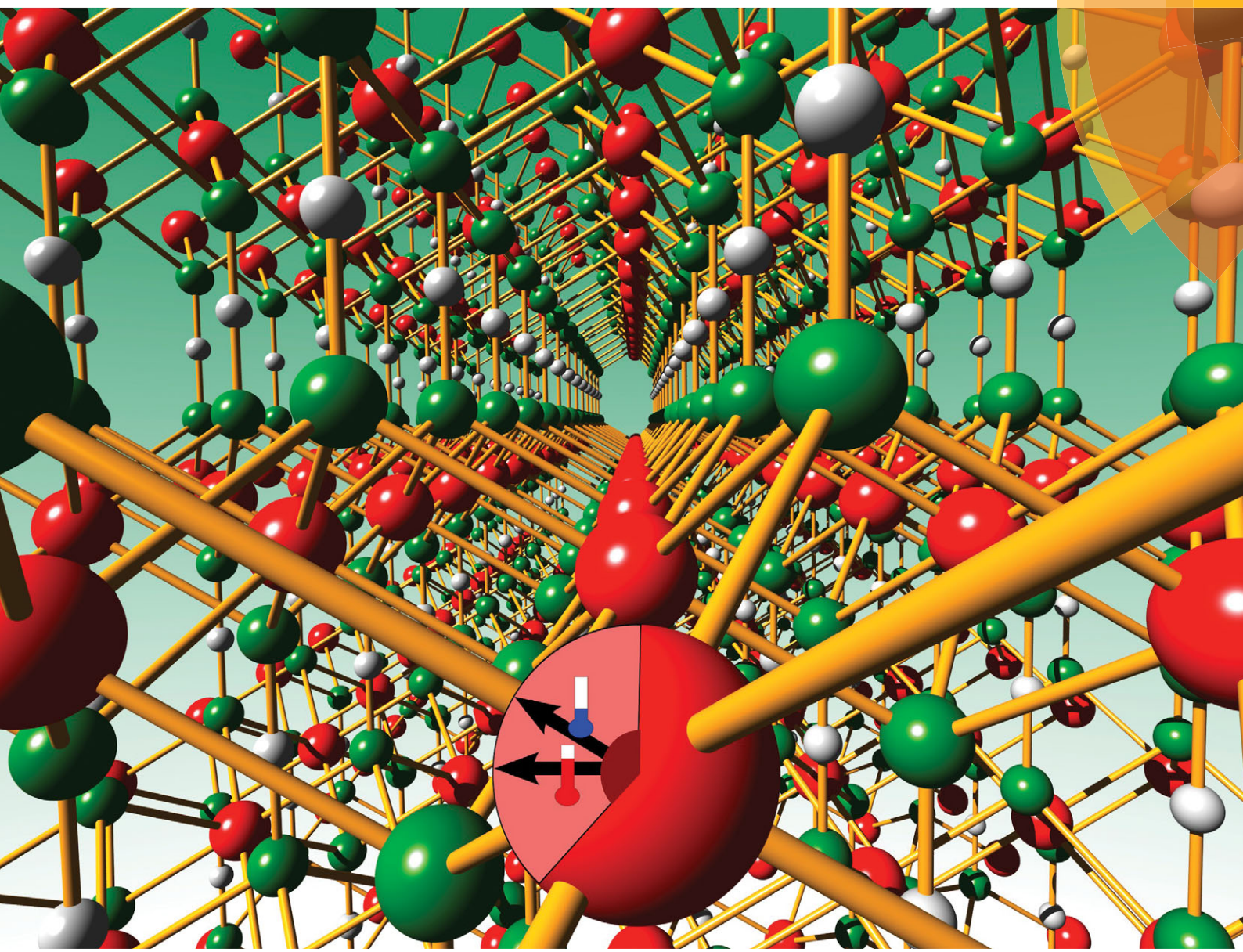

ISSN 1144-0546

ROYAL SOCIETY OF CHEMISTRY

PAPER

M. Herlitschke *et al.*

Magnetism and lattice dynamics of FeNCN compared to FeO

cnrs

NJC

PAPER

View Article Online
View Journal | View Issue

Magnetism and lattice dynamics of FeNCN compared to FeO

Cite this: *New J. Chem.*, 2014, **38**, 4670

M. Herlitschke,*[ab] A. L. Tchougréeff,[cd] A. V. Soudackov,[e] B. Klobes,[a] L. Stork,[c] R. Dronskowski[c] and R. P. Hermann[ab]

Three-dimensional non-oxidic extended frameworks offer the possibility to design novel materials with unique properties, which can be different from their oxide analogues. Here, we present first experimental results concerning unusual magnetic properties of FeNCN, investigated using Mössbauer spectroscopy and magnetometry between 5 and 380 K. This study reveals an unconventional behaviour of the magnetic parameters below the Néel temperature of 350 K, *i.e.*, the hyperfine field on iron decreases with decreasing temperature. At room temperature, quadrupole and hyperfine magnetic field interaction energies are comparable in magnitude, which leads to a rare five-line absorption spectrum. We suggest that these features in the hyperfine field are caused by the combination of a small Fermi contact term and a temperature-dependent contribution from the orbital momentum and the dipole term. One additional spectral component is observed, which exhibits a magnetic relaxation behaviour and slows down at low temperatures to yield a sextet. The magnetometry data suggest that the antiferromagnetic FeNCN is rich in structural distortions, which results in a splitting of the field-cooled and zero-field-cooled curves. The lattice dynamics of FeNCN were investigated using nuclear inelastic scattering. The comparison of the obtained data with literature data of iron monoxide reveals very similar iron phonon modes with a small softening and a slightly reduced sound velocity.

Received (in Montpellier, France) 20th January 2014,
Accepted 5th May 2014

DOI: 10.1039/c4nj00097h

www.rsc.org/njc

1 Introduction

The novel magnetic materials *M*NCN (M = metal) are three-dimensional extended frameworks which can be considered as nitrogen containing analogues to the related transition-metal monoxide. In this analogy the NCN^{2-} dianion bridges the metal ions and acts as a diamagnetic ligand supporting the exchange interaction, following the superexchange coupling scenario. The transition-metal monoxides MnO, FeO, CoO and NiO have received much attention in the past due to the origin of their insulating behaviour as Mott-insulators[1] and their antiferromagnetic coupling.[2] Some of these properties are also observed in the corresponding novel non-oxidic frameworks.

The usage of NCN^{2-} as a connecting bridge has a long history, beginning with the fertilizer CaNCN.[3] Investigations of other carbodiimide compounds of alkaline, alkaline-earth metals and other elements followed in the last decades.[3] The investigation of magnetic interactions mediated by such inorganic ligands was initiated more recently. First results were achieved in the field of metal organic frameworks with polymeric metal cyanide compounds, whereby it was found that short bridges (as azido-, cyano- or oxo-bridges) are necessary in order to obtain a strong magnetic coupling between the metal ions.[4,5] Furthermore, magnetic coupling was observed in dicyanamide and tricyanomethanide compounds.[4] In the last decade, different transition metal monoxide analogues bearing the NCN^{2-} bridges were prepared as extended non-oxidic frameworks and characterized structurally and magnetically.[3,6,7] In 2008, the synthesis of FeNCN was reported by Liu *et al.* with first structural and magnetometric investigations.[7,8]

FeNCN crystallizes in the $P6_3/mmc$ (194) space group at room temperature, with completely linear NCN^{2-} bridges.[8] The structure can be seen as alternating Fe^{2+} and NCN^{2-} planes (Fig. 1). The local environment of each iron comprises six nitrogens, coordinating the iron cation in a slightly distorted octahedron with site symmetry $\bar{3}m$. On the other hand, the carbodiimide is found in a trigonal iron prism with a structural motif that resembles the NiAs type. The corresponding Fe–Fe and Fe–N bond lengths are given in Table 1. The first susceptibility measurements revealed a Néel temperature of 345 K.[7] The exchange constants obtained by

[a] *Jülich Centre for Neutron Science JCNS and Peter Grünberg Institute PGI, JARA-FIT, Forschungszentrum Jülich GmbH, D-52425 Jülich, Germany. E-mail: r.hermann@fz-juelich.de; Fax: +49 2461 61-2610; Tel: +49 2461 61-4786*
[b] *Faculté des Sciences, Université de Liège, B-4000 Liège, Belgium*
[c] *Chair of Solid-State and Quantum Chemistry, RWTH Aachen University, D-52056 Aachen, Germany*
[d] *Independent University of Moscow, Moscow Center for Continuous Mathematical Education, Bolshoi Vlasevsky Per. 11, 119002 Moscow, Russia*
[e] *Department of Chemistry, University of Illinois at Urbana-Champaign, Urbana, IL, USA*

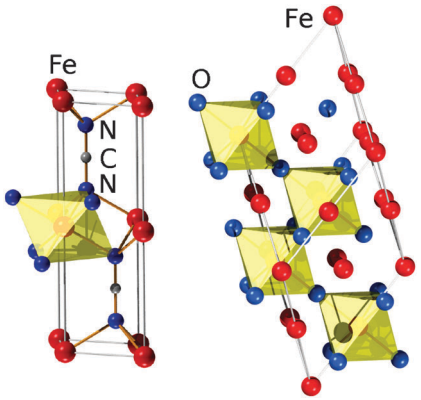

Fig. 1 Structure of FeNCN illustrated in a $P6_3/mmc$ unit cell (left) and FeO in $R\bar{3}$ (right). The octahedral coordination of the iron is depicted for each Wyckoff position.

Table 1 Inter-atomic distances in FeO at 12 K[12] and FeNCN at room temperature[8]

Distance (Å)	FeO	FeNCN
Fe–Fe (same layer)	3.035(6)	3.269(1)
Fe–Fe (adjacent layer)	3.066(6)	4.700(1)
Fe–O/Fe–N	2.15(2)	2.20(2)

density functional calculations (DFT) indicate a weak ferromagnetic coupling of the spins within the iron plane and a leading antiferromagnetic coupling between adjacent planes.[9] Nonetheless, DFT is notoriously unreliable to find the real ground state, also for FeNCN,[10] and DFT exchange parameters have no clear meaning. Many-particle methods are a better choice.[11]

For comparison, the analogous iron monoxide has essentially a defect NaCl structure at room temperature, which distorts rhombohedrally along the [111] direction below the Néel temperature, T_N = 198 K.[14] The crystal structure at 12 K is $R\bar{3}$ (148).[12] The magnetic order is ferromagnetic in the (111) planes but antiferromagnetic with respect to neighbouring planes, with moments pointing in the [111] direction.[14] Stoichiometric FeO is not stable under ambient conditions and thus always cation deficient. Just as for FeNCN, one can more or less artificially represent FeO as a layered structure in the [111] direction (Fig. 1) but containing four different iron sites, with site symmetry $\bar{3}$,$\bar{3}$,$\bar{1}$ and $\bar{1}$, respectively. The local environment of the iron ion is a distorted octahedral coordination by oxygen atoms in each case. The inter-atomic distances for this material are also given in Table 1. In summary, iron monoxide and iron carbodiimide exhibit a similar local iron environment with a mean nearest neighbour distance of about 2.2 Å in an octahedral coordination by oxygen or nitrogen, respectively. Furthermore, both compounds exhibit a similar antiferromagnetic coupling, although the iron–iron distances between adjacent layers are quite different. It is also remarkable that the Néel temperature of the FeNCN is larger than for FeO. This increase in transition temperature sets the iron carbodiimide apart from the manganese, cobalt and nickel carbodiimide, which exhibit a lower transition temperature as compared to the corresponding oxides (see Table 2). Furthermore, the Néel temperature is in the order of the d-shell filling for the oxides but not for the carbodiimides, whose order is broken by FeNCN only. Consequently, stronger exchange interactions might take place in FeNCN or the non-stoichiometry in the metastable FeO causes non-uniformity of the magnetic interaction and leads to the lower transition temperature. However, the iron carbodiimide is thus a particularly attractive target for magnetic investigations using Mössbauer spectroscopy and magnetometry.

Table 2 Transition temperatures of metal oxides and the related carbodiimides

M	M–O^{2-} (K)	M–NCN^{2-} (K)
Mn^{2+}	119[13]	30[3]
Fe^{2+}	198[14]	345[7]
Co^{2+}	289[13]	255[6]
Ni^{2+}	524[13]	360[6]

2 Experimental

2.1 Sample preparation

The sample was prepared as described in ref. 8. In brief, in the first step the reaction of $[Fe(NH_3)_6]^{2+}$ with cyanamide in aqueous solution produces the precursor $Fe(NCNH)_2$. This precursor is air sensitive and must be produced and stored in an inert atmosphere. In the second step, the precursor is decomposed in a halide salt flux at temperatures around 400 °C, thus forming the FeNCN compound plus other by-products. After rinsing with H_2O, the purity was checked with CHN^- analysis and XRD.

2.2 Mössbauer spectroscopy

The Mössbauer spectral data were obtained using a spectrometer operating in constant acceleration mode and using a sodium iodide scintillation detector distributed by Ritverc GmbH. Calibration was performed by a room temperature measurement of an α-Fe foil. Around 30 mg of the powder sample were mixed with boron nitride and fixed with tape, for measurements below 300 K, or aluminium foil, for measurements above 300 K, in a titanium sample holder. A small Fe impurity of the aluminium foil was pre-characterized and taken into account in the subsequent data analysis. The sample was mounted into a Janis Research SHI-850-5 cryostat. The temperature steps for the measurement were chosen with monotonic temperature variation in order to avoid hysteresis effects. Representative spectra are depicted in Fig. 2. The data were analysed using a program based on the Liouville operator formalism and a stochastic relaxation model.[15,16]

2.3 Magnetometry

Macroscopic magnetisation measurements were carried out using the vibrating sample magnetometry (VSM) option of a Cryogenic Ltd. closed cycle measurement system. Field-cooled (FC) and zero-field-cooled (ZFC) measurements in the range of ±10 T and 5–300 K were recorded. Additional ZFC/FC measurements between 5 and 400 K in the range of ±2 T were carried out on the VSM option of a physical property measurement

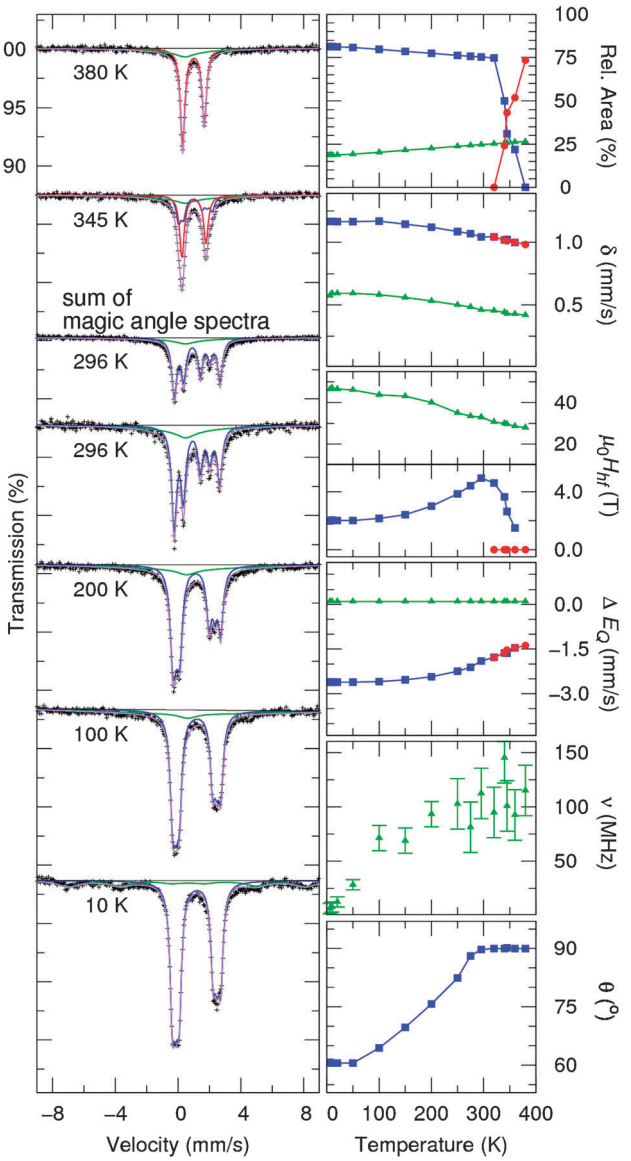

Fig. 2 Mössbauer spectra of FeNCN at selected temperatures and the extracted parameters from all measurements. The non-relaxing component, attributed to stoichiometric FeNCN, is depicted in blue for the magnetically ordered phase and in red for the paramagnetic phase. The relaxing component is depicted in green and the sum of all components in light purple. The relaxation frequency, ν, and the angle, θ, between the hyperfine field and the c axis are plotted only for components with non-vanishing contribution.

system (PPMS) distributed by Quantum Design. All presented data were measured upon heating. The sample was prepared as a powder.

2.4 Nuclear inelastic scattering

Nuclear inelastic scattering (NIS) measurements[17] enable direct access to the iron specific vibrational modes *via* the ^{57}Fe Mössbauer resonance. More details about this technique can be found in ref. 18. The measurements were carried out at beamline P01, PETRA III. Around 12 mg of powderous FeNCN was placed between two tapes. We recorded the NIS spectrum at room temperature. The energy resolution during the experiment was $\approx$0.9 meV. The elastic line and the background were subtracted from the measured NIS spectrum, and the iron partial density of phonon states (DPS) was extracted using the DOS program.[19]

3 Results

3.1 Mössbauer spectroscopy

Prior to modelling, a visual inspection of the Mössbauer data (Fig. 2) reveals four distinct regions in terms of temperature dependence. At high temperatures, above 350 K, the material exhibits a paramagnetic doublet. Below the Néel temperature of $\approx$350 K, a five-peak spectrum is observed with a broad background component. Below 275 K, the hyperfine field, μ_0H_{hf}, of the magnetically split component reduces noticeably from 4.94 T at 296 K to 2.04 T at 10 K. In the last region, below 100 K, the broad component also develops a distinct magnetic splitting.

In order to model the temperature dependence of the spectra, we used a two-component model. One of these components, *i.e.*, the broad one, exhibits a temperature-dependent relaxation process for the magnetic hyperfine interaction, with a relaxation frequency ν. The obtained parameters at selected temperatures are given in Table 3. In order to improve the stability of the model, the spectra were first fitted with the relative area of the two components as free parameters, and subsequently, we introduced a Debye model[20] for the variation of the relative Lamb–Mössbauer factor. Thus, the relative area in the fit is proportional to the relative amount of the component times the Lamb–Mössbauer factor. Later, the calculated values were used as fixed parameters. The relative areas obtained in the first step and the Debye fit of the second step are depicted in Fig. 3. The determined Debye temperatures, or more precisely Mössbauer temperatures Θ_M,[20] and the Lamb–Mössbauer factors f_{LM} at room temperature are Θ_M = 248(4) K and f_{LM} = 0.51(1) for the non-relaxing component and Θ_M = 295(30) K and f_{LM} = 0.62(7) for the relaxing component, respectively.

The non-relaxing component in the measured spectra, component I, was only adjustable with a model that takes into account a non-zero angle θ between the axis of the largest principal component of the electric field gradient and the hyperfine field for all spectra below 350 K. The angle was estimated to be about 90° at room temperature. Considering the three-fold rotation symmetry along the c axis (Fig. 1), it follows that the principal component V_{zz} of the diagonalised electric field gradient tensor must be along c and the asymmetry parameter must be $\eta = |V_{yy} - V_{xx}|/V_{zz} = 0$.

Table 3 The adjusted parameters from selected Mössbauer spectra. The fixed parameters, according to the description in the text, are given without errors

	χ_{red}^2		Rel. area (%)	δ (mm s^{-1})	ΔE_Q (mm s^{-1})	μ_0H_{hf} (T)	θ (°)	ν (MHz)
380 K	1.31	I	73(4)	0.98(1)	−1.38(1)	—	—	—
		II	27(4)	0.42(—)	0.1(—)	28(—)	—	115(20)
296 K	1.39	I	75(3)	1.04(1)	−1.90(1)	4.94(1)	90(1)	—
		II	25(3)	0.46(—)	0.1(—)	33.1(—)	—	112(20)
10 K	1.83	I	81(1)	1.17(1)	−2.61(1)	2.04(2)	60.5(3)	—
		II	19(1)	0.59(2)	0.1(1)	47.1(5)	—	9(3)

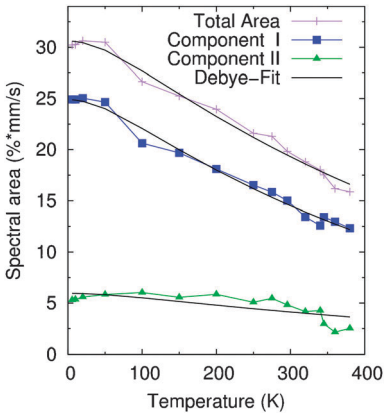

Fig. 3 The spectral area of components I and II in the first step of the fitting procedure and the corresponding Debye fits used for the second step.

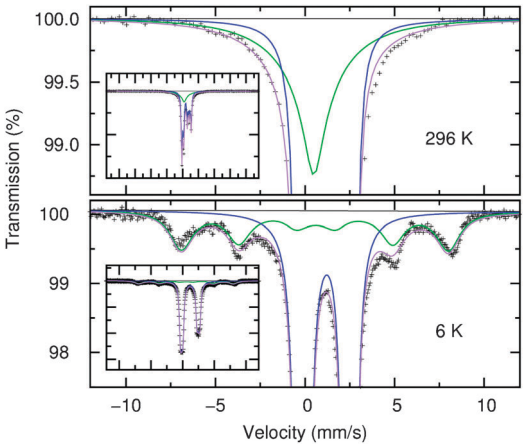

Fig. 4 Additional spectra of FeNCN at room temperature with enlarged velocity range (top) and 6 K measurement with very good statistics (bottom). The colors are chosen as in Fig. 2.

Accordingly, the hyperfine field must be in the *ab* plane at this temperature. The angle θ decreases with decreasing temperature to $\theta = 60^\circ$ at 10 K. This angle corresponds to the angle between the Fe–N bond and the *c* axis. Close to the magnetic transition, *i.e.*, above 320 K, the parameter θ needed to be fixed to 90° in order to obtain a reliable adjustment.

At room temperature, an isomer shift, δ = 1.04 mm s^{-1}, characteristic of high-spin Fe^{2+} is obtained for component I. This isomer shift is thus quite similar to wüstite with $\delta \approx 0.95$–1.02 mm s^{-1},[21] although the local environment is modified from an oxygen to nitrogen coordination but with similar symmetry. The measured isomer shift is given by the sum of the genuine isomer shift and a relativistic correction, called second-order Doppler shift. The temperature behaviour of the isomer shift was fitted within the Debye model.[20] A Mössbauer temperature for the second-order Doppler shift[20] of 451(30) K was obtained. The observed hyperfine magnetic field exhibits a remarkable behaviour, it increases below the Néel temperature, reaches a maximum at ≈300 K and then starts to decrease. Furthermore, the maximum at 5 T is also quite small for usual solids. We attribute component I to the stoichiometric FeNCN material. Note that component I shows a slightly broadened linewidth of ≈0.35 mm s^{-1} at all temperatures, a broadening that could indicate small deviations in the local environment of the iron ion.

The broad, relaxing component, component II, features an isomer shift of roughly 0.6 mm s^{-1} at 10 K indicating Fe^{3+} or low spin Fe^{2+}. The hyperfine field of 47 T at 10 K is characteristic for Fe^{3+}. It was only possible to extract reliable values for the quadrupole interaction and the hyperfine field of component II below 100 K, due to the smearing effect of the relaxation process and the correlation of the hyperfine field with the relaxation frequency. Above 100 K, the isomer shift for component II was calculated using the Debye model with the Mössbauer temperature extracted from the isomer shift of component I. The hyperfine field was extrapolated linearly and the quadrupole interaction was kept fixed. In the final step, all fits were re-adjusted with the hyperfine field as a free parameter but with a fixed relaxation frequency. In order to verify our modelling of this component, we measured the room temperature spectrum of FeNCN with an enlarged velocity range (Fig. 4, top) and found that component II gives contributions to the absorption spectra up to a velocity of ±8 mm s^{-1}, which evidences the large area occupied by component II compared to component I.

The used stochastic relaxation model[16] for component II was chosen phenomenologically in order to describe this component, whereby the difference between a relaxation parallel or perpendicular to the electric field gradient cannot be resolved due to the quadrupole interaction of ≈0 mm s^{-1}. A measurement at 6 K with very good statistics of ≈6 million counts in the baseline, *i.e.*, roughly ten times the usual number of counts in the baseline of our measurements, reveals some discrepancies with the used model (Fig. 4, bottom). These discrepancies could be related to a slightly different relaxation mechanism, some additional distribution of hyperfine parameters or another component.

Both components exhibit texture at all temperatures, *i.e.*, preferential orientation. The texture was verified using a magic angle measurement[22] (see Fig. 2). A small discrepancy between the fit and the spectra at about 4 mm s^{-1} can be observed at any temperature, possibly related to an incremental increase in the linewidth. We found no indication for this discrepancy to results from an additional component.

3.2 Magnetometry

The ZFC/FC curves at different magnetic fields are plotted in Fig. 5a and feature an antiferromagnetic transition close to 350 K, as also observed by Mössbauer spectroscopy. The splitting in the ZFC/FC curves below 350 K for the three different applied fields can be an indication of different magnetic order phenomena. In principle, this splitting could be related to superparamagnetism which would also explain the relaxation behaviour observed for component II by Mössbauer spectroscopy. However, superparamagnetism is ruled out because the splitting also appears at a magnetic field of 2 T and at such high fields the order should vanish. The ZFC/FC splitting could also

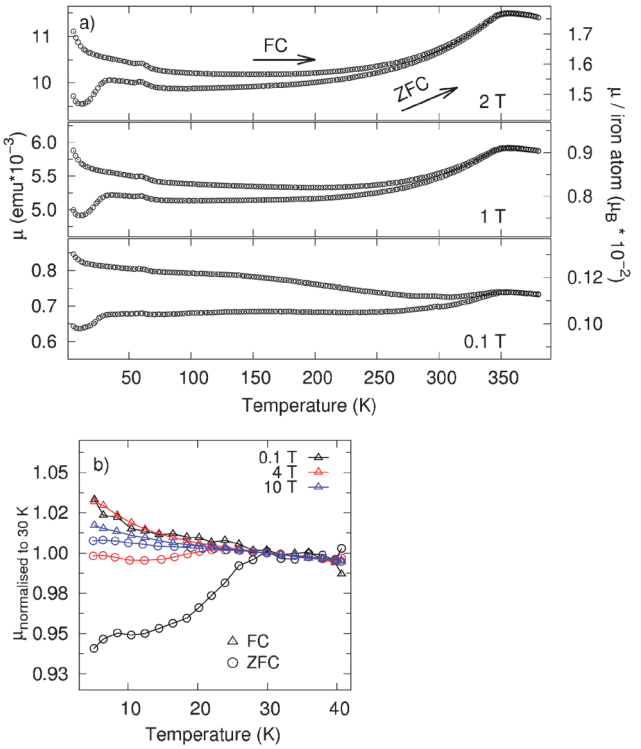

Fig. 5 Temperature dependence of the magnetic moment μ in FeNCN for ZFC/FC measurements with different magnetic fields. The temperature was varied between 5 and 380 K for (a) and between 5 and 40 K for (b).

be related to a spin-glass. But, similarly to superparamagnetism, the spinglass is a ''weak'' magnetic order and a shift in transition temperature with increasing magnetic field, until it vanishes or smears out at high fields,[23,24] would be expected. No change in transition temperature was observed and the transition becomes gradually even more pronounced with increasing field. Other frequency dependent order phenomena can also be ruled out, because the transition temperatures in Mössbauer spectroscopy and magnetometry are very close and both measurements provide information at very different time scales, ns and s, respectively.

We suggest to attribute the splitting of the curves to distortions in the sample, as reported for YFe_2O_{4-x}.[25] The structural disorder due to distortions or impurities locally destroys the antiferromagnetic order and leads to parasitic ferrimagnetic moments. As a consequence, the moments in the sample will arrange and ''freeze'' differently upon zero-field cooling compared to field cooling, because the introduced parasitic moments align parallel to the applied field and generate completely different starting conditions for the cooling procedures. A microscopic description of similar behaviour can be found for diluted antiferromagnets in a uniform field (DAFF), based on a random field Ising model.[26–28] The interplay of the anisotropy and dilution (impurities) also leads to different behaviour on ZFC or FC.

Another feature of the data in Fig. 5a is the small bump at around 60 K. This peak is related to the freezing of oxygen. It was not possible to remove this peak with additional purging. Consequently, there is a strong adsorption of oxygen on the surface, according to our experience.

With respect to component II in Mössbauer spectroscopy two conclusions can be drawn from the magnetometry data: first, there is no remarkable indication for typical oxides, *e.g.*, Verwey transition for magnetite at 119 K or Néel temperature for wüstite at 198 K. Second, the overall magnetisation up to 2 T is very small and with a contribution of almost 19% of component II, estimated by Mössbauer spectroscopy, one would expect much higher values considering ferri- or ferromagnetic materials. As a consequence, only antiferromagnetically coupled iron containing compounds or impurities are reasonable for component II.

Beside the Néel transition at 350 K another transition was found only in the ZFC curves in the range of 5–30 K, a transition which also features an interesting field-dependent behaviour. ZFC/FC measurements up to 10 T in the range of 5 to 40 K exhibit a splitting between both curves, see Fig. 5b. The existence of this splitting up to high magnetic fields indicates a very strong order. This effect may be related to some unreacted $Fe(NCNH)_2$ precursor, which is known to exhibit similar behaviour in low temperature magnetometry (supporting information in ref. 8). Furthermore, in Mössbauer spectra we observed a magnetic transition of the precursor from a paramagnetic to an ordered state between 15 and 30 K (detailed investigations will be reported elsewhere). This transition could lead to the observed field-dependent splitting of ZFC/FC curves between 5 and 30 K. $Fe(NCNH)_2$ is not observed in the Mössbauer spectra, but a small amount of $\approx$1% can not be excluded. Magnetometry might be sensitive to the latter material, because the paramagnetic $Fe(NCNH)_2$ provides a larger signal at low temperatures compared to the antiferromagnetic FeNCN.

3.3 Nuclear inelastic scattering

The extracted iron specific density of phonon states (DPS) of FeNCN, $g(E)$, is depicted in Fig. 6. In both compounds, the iron monoxide and the iron carbodiimide, the major number of iron phonon states is located in the energy region below 40 meV with similar shape in each case. The maxima of FeNCN are slightly shifted towards lower energy as compared to FeO, which represents relatively softer phonon modes. The features in the FeNCN spectrum are more defined compared to FeO, probably due to a better resolution in our experiment.

In the low energy region, between 4 and 8 meV, iron carbodiimide features an increased number of phonon states, as seen in the reduced DPS, *i.e.*, $g(E)/E^2$. This bump is specific for FeNCN and not obvious in FeO and might be an indication of glass-like behaviour. The area of the bump compared to the overall DPS is about 0.8(4)%. The Debye level of FeNCN, defined as the low energy limit

$$\lim_{E\to 0}\frac{g(E)}{E^2},$$

seems to be slightly increased as compared to FeO. This increase corresponds to a decrease of the sound velocity.[30] The exact determination of the Debye level is quite difficult,

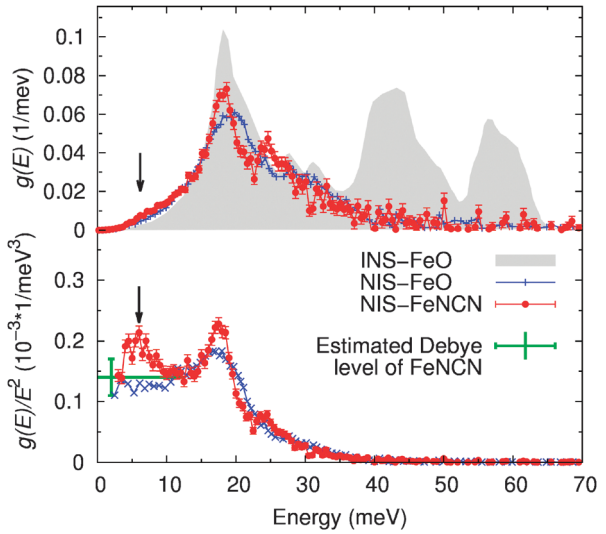

Fig. 6 Iron specific DPS (top) and reduced DPS (bottom) of FeNCN extracted from NIS measurements at 300 K compared with FeO at 0.9 GPa from ref. 29. In addition, the total DPS of FeO obtained from inelastic neutron scattering (INS) (ref. 14) is highlighted in grey. The region of the subtracted elastic line was omitted in the reduced DPS plot.

Table 4 The calculated values from the iron specific DPS of FeNCN, obtained using the DOS program[19]

Lamb–Mössbauer factor	0.62(4)
Internal energy	91(10) meV
Mean force constant	127(60) N m^{-1}

due to the presence of the soft phonon mode, the finite resolution and the subtraction of the elastic line. In approximation, one can confine the possible range of the Debye level as highlighted in Fig. 6. This range leads to a sound velocity of 3200 m s^{-1} ± 300 m s^{-1}. For comparison, iron monoxide has a sound velocity of around 3500 m s^{-1} as determined by NIS.[30] A list of other parameters calculated using the extracted DPS from the NIS measurement of FeNCN at room temperature is given in Table 4.

4 Discussion

Investigation of iron carbodiimide revealed some similarities to the metastable iron monoxide, as expected. The isomer shift is comparable to the iron monoxide with the same Fe^{2+} state and a similar AF order appearing at higher temperatures. In contrast, the hyperfine field is strongly reduced from 34 T in the iron monoxide at 77 K[21] to *ca.* 2 T for FeNCN.

The second component with a relative contribution of ≈19% in Mössbauer spectra exhibits an isomer shift of 0.6 mm s^{-1} and a hyperfine field of 47 T at 10 K. This combination of hyperfine parameters is characteristic of Fe^{3+}. The hyperfine field is in the usual range for iron oxides and hydroxides. The magnetometry data reveal only a small magnetic moment for all temperatures and we found no indication in the magnetometry measurements for this component to be a common oxide (see Fig. 5). We assume that component II is an impurity, related to the production or ageing process of FeNCN or the $Fe(HNCN)_2$ precursor. The magnetic order of this impurity at low temperatures indicates a quite stoichiometric material. The overall small magnetisation at low temperatures and high magnetic fields leads to the conclusion of a strong antiferromagnetic or weak ferri/ferromagnetic coupling. Furthermore, an intrinsic distribution of the Fe^{3+} impurity could explain the splitting in ZFC/FC curves below the Néel temperature.

Another remarkable difference between FeO and FeNCN is an unusual behaviour of the hyperfine magnetic field in component I. Usually, a decrease of the hyperfine field with increasing temperature is observed until the hyperfine field vanishes at the Néel or Curie temperature, as indeed observed for FeNCN, but only between 300 and 350 K. Below 300 K the hyperfine field in FeNCN decreases with decreasing temperature. In addition, the angle between the hyperfine field and the quadrupole interaction gradually decreases from 90° to 60° between 300 and 10 K. This change in the angle corresponds to an alignment of the hyperfine field in the *ab* plane at room temperature and a 60° tilting with respect to the *c* axis at low temperatures, assuming the $P6_3/mmc$ structure. The low temperature angle is thus equal to the angle between the Fe–N bond and the *c* direction. Both, the change of the hyperfine field and the change of the angle θ, exhibit a similar behaviour upon changing the temperature and thus are likely correlated. In order to improve the understanding of the observed behaviour of component I possible interactions in the material must be discussed in light of the magnetometry results and the antiferromagnetic order at low temperatures.

First, while analysing the Mössbauer data, a magnetic relaxation scenario according to ref. 15 and 16 was tested in order to explain the observed reduction of the hyperfine field of component I. Two facts contradict this hypothesis: the relaxation does not reproduce the correct line shape, *i.e.*, the observed high velocity lines in the low temperature spectra are broader than the low velocity lines but relaxation tends to make them equal. Furthermore, the relaxation frequency would increase upon decreasing the temperature in contrast to usual observations.

Second, we consider that the magnetic field seen in the nucleus is reduced upon decreasing the temperature. The hyperfine magnetic field in the absence of an external field is defined as:[31]

$$\mu_0 H_{hf} = B_D + B_L + B_S$$

with the contributions B_D produced from the dipolar interaction, B_L produced from the electronic orbital momentum and B_S related to the Fermi contact term. The first two terms are usually small in iron compounds[31] and thus we first focus on the Fermi contact term, which describes the interaction of s-electrons with the nucleus. Because the s-electrons are paired, their contribution is due to their polarization by d-electrons and is quite large.[32] Consequently, possible effects of d-electron configuration need to be considered as they may change the contribution of the Fermi contact term.

One possibility is that the octahedral environment of the iron ion in combination with the high-spin state produces a – potentially dynamic – Jahn–Teller effect. We thus have to determine the electronic ground state of the d-shell. The Fe^{2+} ion in the trigonally distorted octahedral environment formed by the NCN^{2-} groups, as depicted in Fig. 1, has been employed as input for the Effective Hamiltonian Crystal Field (EHCF) method.[33,34] This calculation reveals the ground state of the Fe^{2+} ion to be high-spin, in agreement with previous calculations[11] and the observed isomer shift. The octahedral environment leads to the $^5T_{2g}$ ground state. The trigonal distortion of the octahedral field, induced by the NCN units, further splits this state to the $^5A_1$ state and the spatially degenerate ^5E states. Our calculation by the EHCF method shows that the true ground state is precisely the spatially non-degenerate $^5A_1$ state, in agreement with the negative sign of the quadrupole interaction as also outlined in ref. 31. In the case of a ^5E ground state, the quadrupole interaction would be positive. The ^5E state is estimated to be 320 K above the ground state. Although this calculation is close to the border of its precision, it may indicate a possible thermal population of the ^5E states. This thermal population is directly seen in the temperature dependence of the quadrupole interaction. An estimation of the temperature-dependent quadrupole interaction according to the Ingalls model,[35] with or without lattice contribution, leads to a splitting between the $^5A_1$ and ^5E states ranging between 500 and 900 K. Due to the $^5A_1$ ground state and the absence of any step-like change[36] in isomer shift or quadrupole splitting a (dynamic) Jahn–Teller effect can be ruled out.

Another possibility to consider is a high-to-low spin transition. We found no indication of such a transition,[20] because the isomer shift changes smoothly and no step-like change was observed. Also the Mössbauer temperature for the second order Doppler-shift of 451(30) K is reasonable and does not indicate any strong change.

In summary, a transition within the d-orbitals, which would lead to the observed behaviour of the hyperfine field, and the angle θ is thus quite unlikely. However, the covalency of the Fe–N bond was not considered so far. Because the electronegativity of N as compared to O is closer to iron, the bond will be more covalent and a stronger super-exchange is expected.[37,38] Thus the covalency could be a reason for the large Néel temperature of FeNCN as compared to FeO but it does not explain the exceptional behaviour of iron within the *M*NCN series, since the bonding character in the series should be the same. A second consequence of the increasing covalency is a reduction of the Fermi contact term.[39,40] This reduction might explain the exceptionally strong reduction in the hyperfine field of component I as compared to iron oxide. The theoretical value of the Fermi contact field would be 11 T per spin[41] leading to 44 T for Fe(II) high spin. The observed hyperfine field of component I is around 2 T at low temperatures and thus indicates a remarkably small reduction parameter[39,40,42] of $\kappa = \frac{H_{\text{observed}}}{H_{\text{theoretical}}} = 0.05$.

Consequently, the previously ignored spin dipole and orbital momentum terms need to be considered for the temperature behaviour of the hyperfine field, as they might have a similar magnitude to the Fermi contact term. Both terms can change with temperature and thus may explain the temperature behaviour of the hyperfine field. By assuming similar asymmetries for the charge density and the spin density, the dipolar interaction term can be described as[41,43] $|B_D| = \mu_B V_{zz} e$. The orbital momentum term will be zero at low temperatures due to the nondegeneracy of the $^5A_1$ state, *i.e.*, the orbital quenching. With increasing temperature, the ^5E state will be populated due to thermal excitation. This scenario can be observed in the strong temperature dependence of the quadrupole interaction, which is directly linked to the thermal population of these levels.[35] The sum of the arising orbital momentum term and the dipole term change the hyperfine magnetic field by around 3 T between 10 K and room temperature, assuming that the Fermi contact term stays constant. Above room temperature, the total field drops again due to the vanishing sublattice magnetisation at the Néel temperature.

The interplay between the hyperfine field contributions could also explain the observed change in the angle θ, under the assumption that the low temperature field, likely oriented at 60° from the *c*-axis, and the temperature dependent orbital and dipolar terms are not (anti-)parallel. Furthermore, the larger T_N in FeNCN as compared to other metals could also be related to the arising orbital momentum. This mechanism is not possible for all NCN compounds, because Mn^{2+} is a $3d^5$ system and has a singlet ground state, thus no orbital momentum can be formed, likewise for Ni^{2+} with filled t_{2g} levels. However, for Co^{2+} the Jahn–Teller effect or orbital momentum are possible and the transition temperature in CoNCN is also quite high, close to the related oxide.

The suggested model implies a change of the total atomic moment in size and direction with changing temperature. This hypothesis cannot be verified directly by magnetometry due to the antiferromagnetic order. Further experiments have to be performed in order to gain a deeper insight, such as magnetic structure refinement of neutron diffraction data, absorption spectroscopy, and also high resolution temperature-dependent X-ray diffraction in order to check for any structural distortion that might occur.

5 Conclusion

We have presented measurements of FeNCN, featuring similarities and differences to the related iron monoxide. The Mössbauer spectroscopic data exhibit the same Fe^{2+} state for iron with a similar octahedral coordination environment but with a completely different and unconventional temperature behaviour of the hyperfine field, it decreases upon lowering the temperature. Furthermore, a temperature-dependent reorientation of the hyperfine magnetic field direction from 90° at room temperature to 60° at 6 K was observed, with respect to the *c* axis. Both observed phenomena are likely correlated due to the qualitatively similar behaviour. A study of different possible effects on the d-orbitals leads to the conclusion that an interplay between a strongly reduced hyperfine field and a temperature-dependent

dipole and orbital momentum contribution to the hyperfine field can explain the observed behaviour.

The extracted DPS from the NIS data of FeNCN has a similar shape as compared to FeO due to the similar local environment and the similar bonding, but exhibits a softening with a low-energy phonon mode between 4 and 8 meV. The obtained Debye level of FeNCN is similar to literature values of FeO, however slightly increased. The magnetometry data reveal a Néel temperature of $\approx$350 K and exhibit a splitting of the ZFC/FC curves between Néel temperature and 5 K, this splitting might indicate impurities in the antiferromagnetic order.

Acknowledgements

We are grateful to O. Petracic, M. Angst, A. Houben, G. Long and F. Grandjean for the helpful discussions. We would like to thank H. Sawinski for additional information on the XRD pattern of the reported materials. We acknowledge the Helmholtz Association of German Research Centers for funding VH NG-407 ''Lattice dynamics in emerging functional materials''. Portions of this research were carried out at the light source PETRA III at DESY, a member of the Helmholtz Association (HGF). We would like to thank I. Sergueev, H.-C. Wille, and K. Schlage for assistance in using beamline P01 and for support in analysing the NIS data. This work was performed with a partial support from the Russian Foundation for Basic Research extended through the grant Nr. 14-03-00867.

References

1 K. Terakura, T. Oguchi, A. R. Williams and J. Kübler, *Phys. Rev. B: Condens. Matter Mater. Phys.*, 1984, **30**, 4734.
2 B. Koiller and L. M. Falicov, *J. Phys. C: Solid State Phys.*, 1975, **8**, 695.
3 X. Liu, M. Krott, P. Müller, C. Hu, H. Lueken and R. Dronskowski, *Inorg. Chem.*, 2005, **44**, 3001.
4 C. Janiak, *Dalton Trans.*, 2003, 2781.
5 O. Kahn, J. Larionova and L. Ouahab, *Chem. Commun.*, 1999, 945.
6 M. Krott, X. Liu, B. P. T. Fokwa, M. Speldrich, H. Lueken and R. Dronskowski, *Inorg. Chem.*, 2007, **46**, 2204.
7 X. Liu, R. Dronskowski, R. K. Kremer, M. Ahrens, C. Lee and M.-H. Whangbo, *J. Phys. Chem. C*, 2008, **112**, 11013.
8 X. Liu, L. Stork, M. Speldrich, H. Lueken and R. Dronskowski, *Chem. – Eur. J.*, 2009, **15**, 1558.
9 A. Tsirlin, K. Koepernik and H. Rosner, 2011, ArXiv e-prints, 1106.3665.
10 H. Xiang, R. Dronskowski, B. Eck and A. L. Tchougréeff, *J. Phys. Chem. A*, 2010, **114**, 12345–12352.
11 A. L. Tchougréeff and R. Dronskowski, *J. Phys. Chem. A*, 2011, **115**, 4547–4552.
12 H. Fjellvaag, F. Gronvold, S. Stolen and B. Hauback, *J. Solid State Chem.*, 1996, **124**, 52.
13 G. Srinivasan and M. Seehra, *Phys. Rev. B: Condens. Matter Mater. Phys.*, 1983, **28**, 6542.
14 G. Kugel, C. Carabatos, B. Hennion, B. Prevot, A. Revcolevschi and D. Tocchetti, *Phys. Rev. B: Solid State*, 1977, **16**, 378.
15 M. Blume, *Phys. Rev.*, 1968, **174**, 351.
16 S. Dattagupta and M. Blume, *Phys. Rev. B: Solid State*, 1974, **10**, 4540.
17 W. Sturhahn, T. Toellner, E. Alp, X. Zhang, M. Ando, Y. Yoda, S. Kikuta, M. Seto, C. Kimball and B. Dabrowski, *Phys. Rev. Lett.*, 1995, **74**, 3832–3835.
18 R. Röhlsberger, *Nuclear Condensed Matter Physics with Synchrotron Radiation*, Springer, 2004.
19 V. Kohn and A. Chumakov, *Hyperfine Interact.*, 2000, **125**, 205.
20 P. Gütlich, E. Bill and A. X. Trautwein, *Mössbauer Spectroscopy and Transition Metal Chemistry*, Springer, 2011.
21 N. Greenwood and A. Howe, *J. Chem. Soc., Dalton Trans.*, 1972, 110.
22 J. M. Greneche and F. Varret, *J. Phys. C: Solid State Phys.*, 1982, **15**, 5333.
23 J. A. Mydosh, *Spin Glass*, Taylor & Francis, 1993.
24 M. J. Benitez, O. Petracic, E. L. Salabas, F. Radu, H. Tysz, F. Schth and H. Zabel, *Phys. Rev. Lett.*, 2008, **101**, 097206.
25 M. Inazumi, Y. Nakagawa, M. Tanaka, N. Kimizuka and K. Siratori, *J. Phys. Soc. Jpn.*, 1981, **50**, 438.
26 T. Nattermann, *Spin Glasses And Random Fields: Series on Directions in Condensed Matter Physics*, 1997, vol. 12, p. 277.
27 S. Fishman and A. Aharony, *J. Phys. C: Solid State Phys.*, 1979, **12**, L729.
28 F. Monenegro, S. Rezende and M. Coutinho-Filho, *Rev. Bras. Fis.*, 1991, **21**, 192.
29 V. Struzhkin, H. Mao, J. Hu, M. Schwoerer-Böhning, J. Shu and R. Hemley, *Phys. Rev. Lett.*, 2001, **87**(25), 255501.
30 M. Hu, W. Sturhahn, T. Toellner, P. Mannheim, D. Brown, J. Zhao and E. Alp, *Phys. Rev. B: Condens. Matter Mater. Phys.*, 2003, **67**, 094304.
31 in *Mössbauer Spectroscopy Applied to Inorganic Chemistry*, ed. G. J. Long, Plenum Press, 1984.
32 R. Sternheimer, *Phys. Rev.*, 1952, **86**, 316–324.
33 A. Soudackov, A. Tchougreeff and I. Misurkin, *Theor. Chim. Acta*, 1992, **83**, 389–416.
34 A. Soudackov and K. Jug, *Int. J. Quantum Chem.*, 1996, **62**, 403.
35 R. Ingalls, *Phys. Rev.*, 1964, **133**, A787–A795.
36 M. Tanaka, T. Tokoro and Y. Aiyama, *J. Phys. Soc. Jpn.*, 1966, **21**, 262–267.
37 T. R. Waite, *J. Chem. Phys.*, 1960, **33**, 256–265.
38 J. B. Goodenough and A. L. Loeb, *Phys. Rev.*, 1955, **98**, 391–408.
39 J. Henning, *Phys. Lett. A*, 1967, **24**, 40–42.
40 W. T. Oosterhuis and G. Lang, *Phys. Rev.*, 1969, **178**, 439–456.
41 N. N. Greenwood and T. C. Gibb, *Mössbauer Spectroscopy*, Chapman and Hall Ltd, 1971.
42 H. Andres, E. L. Bominaar, J. M. Smith, N. A. Eckert, P. L. Holland and E. Mnck, *J. Am. Chem. Soc.*, 2002, **124**, 3012–3025.
43 F. van der Woude, *Phys. Status Solidi B*, 1966, **17**, 417–432.